Numerical study on the influence of fractures and zones of weakness on the flow regime of Larsen Ice Shelf

Henner Sandhäger

Alfred-Wegener-Institut für Polar- und Meeresforschung, Postfach 120161, D-27515 Bremerhaven

Introduction

Direct observations, in-situ measurements, and remote sensing data of many Antarctic ice shelf regions reveal the existence of distinct fractures in the ice bodies. Typical fracture structures are, e.g., surface and bottom crevasses, inlets of the ice front, rifts, or shear zones where the surface is highly fractured and broken. Since these fractures represent anomalies in the ice shelf geometry and dynamics, they affect the local glacial conditions to a considerable extent. In numerous cases (e.g., in the case of elongated shear zones or large crevassed areas) significant influence even on the large-scale flow regime of the ice masses can be assumed. This directly leads to the question to what extent such effects have to be captured by numerical flow models used for high-accuracy simulations of ice shelf dynamics.

In the following, first results of a corresponding modelling study of the Larsen Ice Shelf (LIS) are presented. Initially, a reference run was carried out with an 'ordinary' flow model based on the generally used continuum-mechanical approach. Since this simulation of the ice shelf dynamics turned out to be less satisfying, an expanded flow model was additionally applied in which newly developed parameterisations are implemented. These parameterisations describe a localised disintegration of the mechanical integrity of the ice body and the associated dynamical decoupling of adjacent ice shelf parts up to a certain amount. The whole model expansion is based on the hypothesis that deep-reaching zones of weakness exist within the ice shelf. These zones follow the direction of the ice flux and extend from the margins of the glaciers entering the ice shelf up to the calving front.

In order to be able to comprise all three LIS sections 'Larsen A', 'Larsen B', and 'Larsen C' in this modelling effort, their seaward extensions as observed in 1989, 1986, and 1988, respectively, are considered (Fig. 1). However, the dramatic calving and disintegration which occurred afterwards are the focus of future investigations. Associated with regional atmospheric warming and increase in summer melt, these events led to an extensive irreversible retreat of the northern ice shelf areas (Skvarca, 1993; 1994; Vaughan and Doake, 1996; Rott et al., 1996; 1998; Skvarca et al., 1998; 1999; NSIDC, 2002).

Results produced by the 'ordinary' ice shelf model

The diagnostic simulation of ice shelf dynamics using the flow model is based on numerical calculations of an approximate solution of two coupled differential equations which describe the distribution of the horizontal ice flow velocity. The differential equations are obtained by combining the continuum-mechanical momentum and mass balance equations with Glen's flow law, the ice shelf approximation (depth-independency of the horizontal velocity component), and the incompressibility condition. With regard to a regular Cartesian x, y, z-coordinate system, these governing equations of ice shelf flow may be written (e.g., MacAyeal et al., 1986)

$$2\frac{\partial}{\partial x}\left(F\frac{\partial u}{\partial x}\right)+\frac{\partial}{\partial x}\left(F\frac{\partial v}{\partial y}\right)+\frac{1}{2}\frac{\partial}{\partial y}\left(F\left(\frac{\partial u}{\partial y}+\frac{\partial v}{\partial x}\right)\right)=gG_x \quad \text{and} \tag{1}$$

$$2\frac{\partial}{\partial y}\left(F\frac{\partial v}{\partial y}\right)+\frac{\partial}{\partial y}\left(F\frac{\partial u}{\partial x}\right)+\frac{1}{2}\frac{\partial}{\partial x}\left(F\left(\frac{\partial u}{\partial y}+\frac{\partial v}{\partial x}\right)\right)=gG_y \tag{2}$$

with $F=F(u,v,H,A(T),n,m(T_s))$ and $G_{x,y}=G_{x,y}(\rho,h,H)\overset{\rho=\rho_c}{=\!=}H\rho_c(\partial h/\partial x,y)$,

where $\boldsymbol{u}=(u,v)$ is the horizontal velocity vector, H the ice thickness, h ice surface elevation above sea level, ρ density of the ice body, g acceleration due to gravity, T ice temperature, and T_s the mean annual surface temperature. The parameters $A(T)$, n, and m of Glen's flow law are predetermined as follows: the flow factor

$A(T)$ as recommended by Paterson (1994); the exponent $n = 3$; the enhancement factor $m = m(T_s) \equiv 0.9 \exp(0.17 (T_s + 10))$. The temperature distribution in the ice body is approximated by means of the simple relation $T(\tilde{z}) = (T_s - T_b)(\tilde{z}/H)^{1/3} + T_b$ (instead of solving the heat transfer equation), where $\tilde{z}$ is the elevation above the ice shelf base and T_b the temperature at the base. The stress conditions in the ice body, i.e., the distributions of the horizontal deviatoric stress components τ_{xx}, τ_{yy}, and τ_{xy}, are determined by means of Glen's flow law from the strain rates (gradients of the velocity field). In combination with boundary values (for $\boldsymbol{u}$ at the grounding line; for the horizontal gradients of $\boldsymbol{u}$ at the ice front; for T at the surface and bottom of the ice body), this set of model equations describes the distributions of the relevant ice dynamic quantities u, v, T, τ_{xx}, τ_{yy}, and τ_{xy}, subject to the respective ice body geometry.
The model grid used for the numerical simulations is composed of block-centred cells. Each cell represents a volume element of ice body with a constant base $\Delta x \times \Delta y$ of $1.25\,\mathrm{km} \times 1.25\,\mathrm{km}$ and a height varying with depth level between $0.01\,H$ and $0.2\,H$. The decisive numerical method incorporated into the flow model is a relaxation procedure (cf. Herterich, 1987) which facilitates to calculate iteratively an approximate solution of the governing equations of ice shelf flow (1) and (2) from their finite-difference forms.

The digital geometric models of the LIS, which are needed as input data for the model studies, have been deduced from various data sets. To determine the extensions of the different ice shelf areas, i.e., the courses of grounding line and ice front (cf. Fig. 1), corresponding polygons are available (BAS et al., 1993; IOC et al., 1994). The digital terrain model describing the shape of the ice shelf surface (Fig. 1) arises primarily from interpolation and extrapolation of the data set provided by Bamber and Huybrechts (1996). This new terrain model was combined with the BEDMAP ice thickness model (Lythe et al., 2001) to get a hydrostatic relation for LIS. This relation, in turn, allowed a direct conversion of the terrain model into the corresponding digital ice thickness model.

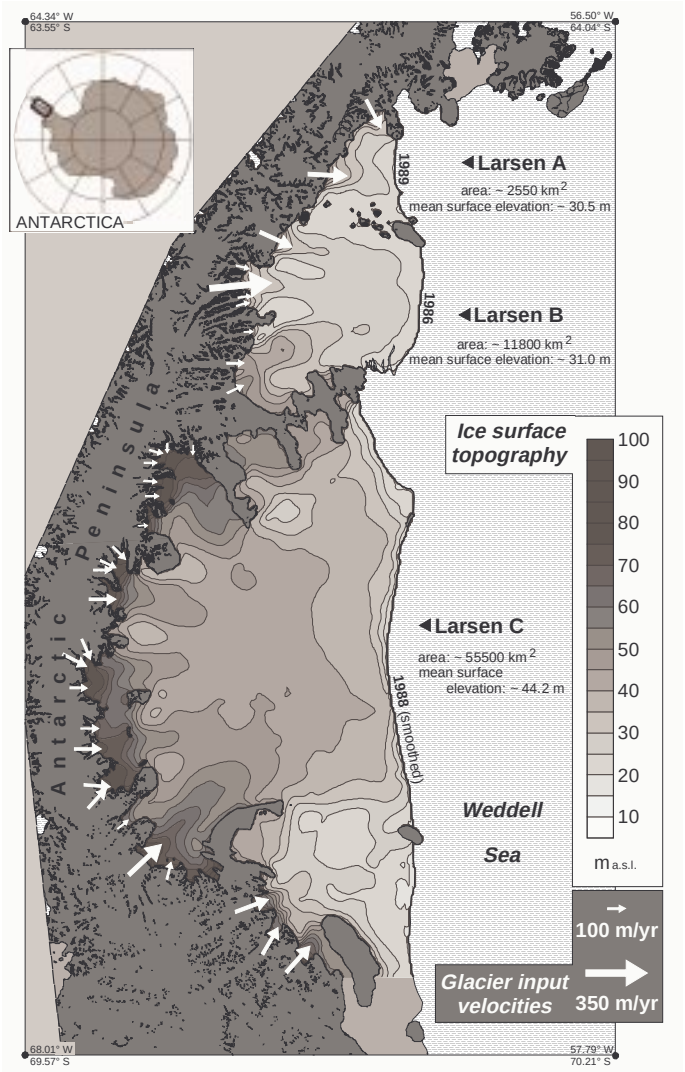

Figure 1: Map of the Larsen Ice Shelf showing the specifications of essential input quantities for the numerical simulations. The quantities are the ice shelf surface topography, the course of the grounding line, the seaward extensions of the different ice shelf areas, and the horizontal velocities of the glacier outflows. A constant speed of $5\,\mathrm{m\,a^{-1}}$ is specified at all passive grounding line sections, where the ice discharge from inland is comparatively small. (Base of map: BAS et al., 1993; 1998; IOC et al., 1994)

A relatively accurate quantification of grounding zone positions and widths of the numerous glaciers draining into the ice shelf regions was obtained using data sets for various surface features (BAS et al., 1993; 1998). In contrast, the determination of glacier inflow velocities (Fig. 1), which are needed as boundary values for the ice shelf model, is largely based on rough estimates (inflow velocities at Larsen A and Larsen B grounding lines were adopted from Bindschadler et al. (1994), Doake et al. (1998), and Scambos et al. (2000)). Model boundary values for the mean annual surface temperature were chosen according to the distribution represented by Vaughan and Doake (1996).

The reference run carried out with the ordinary ice shelf model yielded as major result the ice flow velocity field displayed in Figure 2. The general structure of the simulated flow regime shows a number of large-scale features which are characteristic for many Antarctic ice shelves. This includes the noticeable increase of speed with decreasing distance from the ice front; the occurrence of velocity maxima at the central calving front of the different ice shelf regions; the restraining effect of prominent inland areas and ice rises on the ice shelf flux; and the rather uniformly changing ice shelf movement within extended areas.

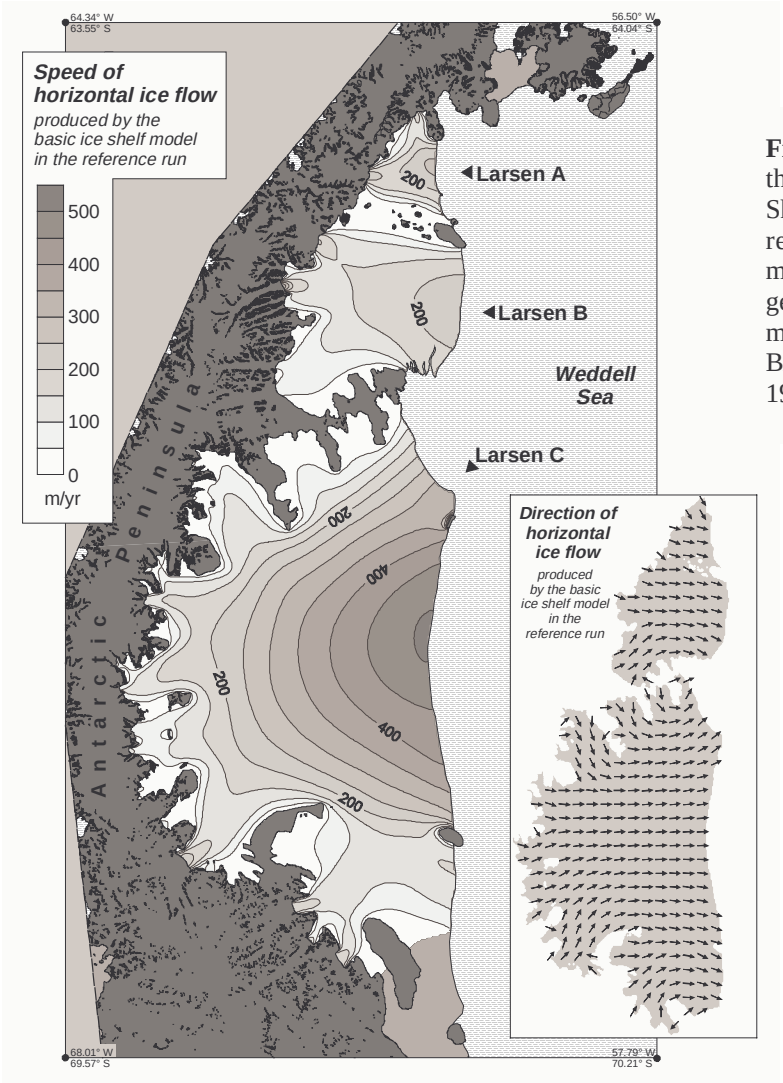

Figure 2: Modelled velocity field of the horizontal Larsen Ice Shelf flow. Shown are the results of the reference run with the ordinary flow model, which is based on the generally used continuum-mechanical approach. (Base of map: BAS et al., 1993; 1998; IOC et al., 1994)

Considerable discrepancies between model results and observed ice dynamic conditions can be ascertained particularly for the near-grounding line areas of LIS. Active grounding line sections are mainly subject to the fast flowing outlet glaciers causing comparatively high ice fluxes, whereas passive grounding line sections are associated with small ice discharge from inland into the ice shelf. According to the frequent alternation between active and passive grounding line sections, an ice flow velocity field structured by distinct small-scale variations can be observed in several LIS regions (cf. Bindschadler et al., 1994; Skvarca, 1994; Rack et al., 1999; 2000). Contrary to that, the numerical simulation yielded for these ice shelf areas – despite

correspondingly chosen boundary values for the horizontal velocities at the grounding line (cf. Fig. 2) – a less differentiated and in comparison to the real situation strongly 'blurred' ice velocity field (Fig. 2). Obviously, the ordinary ice shelf model overestimates the influence of lower ice flow velocities at passive grounding zones on the large-scale flow regime. In addition, it strongly underestimates the influence of the higher velocities at active grounding zones and in ice shelf areas nourished directly via the glacier systems. Consequently, the modelled ice flow speed for the central ice front areas, in particular for those of Larsen B and Larsen C, are about 100 to 200 $m\,a^{-1}$ too small in comparison with observations (Skvarca, 1994; Skvarca et al., 1999; Rack et al., 2000). This 'smearing effect' seems to result mainly from the flow model assumption that the ice shelf body is representing a mechanical entity. This, however, is presumably not the case in such strict manner, at least not in several near-grounding line areas of LIS. In fact, it can be expected that some of the numerous surface features and fractures occurring in these areas (e.g. Bindschadler et al., 1994; Skvarca, 1994; Skvarca et al., 1999; Jezek and RAMP Product Team, 2002) are associated with deep-reaching zones of weakness in the ice body. Hence, its mechanical integrity is partly or even largely disintegrated causing a perceptible ice dynamical decoupling of adjacent ice shelf areas (cf. Rack et al., 2000; Scambos et al., 2000). The question of the possible influence of such structures on the LIS flow regime is, therefore, the main reason for the development and application of an expanded ice shelf model.

Application of the expanded ice shelf model

The expansion of the ordinary ice shelf model is based on the hypothesis (see Fig. 3) that distinct zones of weakness form within the ice body and are important for the flow regime (cf. Rack et al., 2000; Scambos et al., 2000). According to this, the high stress charge of the ice particularly at the margins of the glacier systems causes the formation of deep-reaching crevasses or shear fractures. This happens also at glacier inlet corners, where relatively abrupt transitions from active to passive grounding zones occur. Due to the ice

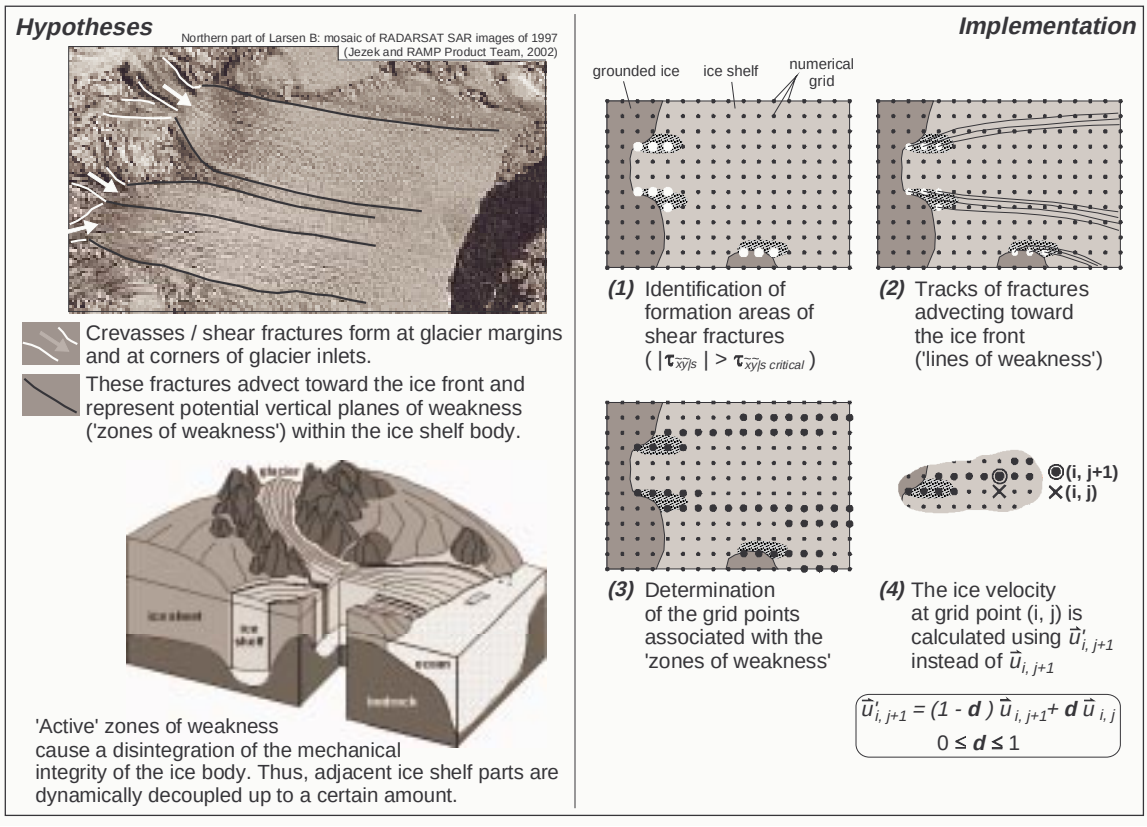

Figure 3: RADARSAT SAR image mosaic of the northern part of Larsen B Ice Shelf (top left; Jezek, K. and RAMP Product Team, 2002) and sketch of a typical glacial system (down left) illustrating the basic hypotheses on the formation of zones of weakness. The right part of the figure indicates, how the initial points and courses of lines and zones of weakness are computed and how the simulation of the dynamical decoupling at such zones is realised (*d* is the degree of decoupling and ***u*** is the horizontal velocity vector).

movement, these features then advect as still active fractures in the off-lying ice shelf areas. Elongated vertical failure plains (zones of weakness) aligned in flow direction form within the ice body and cause an appreciable dynamical decoupling of ice body parts adjoining there. The amount of decoupling depends on the vertical extension of the zones of weakness as well as on the prevailing mechanical and thermal conditions. With increasing degree of decoupling, such zones of weakness can then be seen as significant gradient zones in the velocity field of the corresponding ice shelf body and, thus, contribute to the formation of a heavily differentiated and small-scale structured flow regime.

In order to be able to numerically simulate the possible influence of such hypothetical zones of weakness on the flow of LIS, a parameterisation scheme was implemented in the ice shelf model. This scheme basically comprises four steps (cf. Fig. 3).
The identification of potential formation areas of shear fractures (only these structures are taken into consideration) is performed by analysing the modelled distribution of the stress component $\tau_{\tilde{x}\tilde{y}|s}$, i.e., the horizontal shear stress in the near-surface ice body associated to the local flow direction. Regions in which this stress component exceeds a certain predetermined threshold value $\tau_{\tilde{x}\tilde{y}|s\,critical}$ are then identified as formation areas. However, the fracture processes presumably already take place within the glacier systems. Thus, the threshold value used is suitable for all glacier inlet corners and transitions from active to passive grounding zones to be identified as formation areas of shear fractures. Subsequently, the modelled velocity field is used to compute special flow lines. Along these 'lines of weakness' the shear fractures would be advected from their formation areas to the ice front (note that the time-dependency of these advection processes remains unconsidered). The succeeding discretisation of the lines provides grid points on which a not evanescent degree of decoupling $0 < d \leq 1$ is considered when calculating the velocity vector components (total decoupling corresponds to $d = 1$). The numerical realisation for a selected configuration is shown in Figure 3. However, this approach is numerically stable only for a decoupling lower than 0.8.

Figure 4 shows the distribution of the ice flow speed for LIS simulated with the expanded ice shelf model. A degree of decoupling, $d = 0.63$, was assigned to all considered zones of weakness (cf. inset map in Fig. 4). A comparison with the corresponding results of the reference run (Fig. 2) shows that the newly developed model approach simulates a flow regime of LIS which agrees considerably better with observations and is essentially more plausible from the glaciological point of view. In particular, the complex structure of the ice velocity field near the grounding zones is much better reproduced. Additionally, a reduction of discrepancies between measured and modelled values of the horizontal ice velocities in the central ice front areas is achieved.

The next step to improve the model results could be an optimisation of the predefinition of the two new quantities $\tau_{\tilde{x}\tilde{y}|s\,critical}$ and d representing tuning-parameters of the expanded flow model. Furthermore, a degree of decoupling depending on one or several quantities might be implemented to consider also spatial- and/or time-dependent changes in the mechanical and thermal properties of zones of weakness. Such changes are expected, e.g., as direct consequence of a deactivation of some zones of weakness due to 'healing' or an activation due to additional fracturing, frictional heating, or melt water infiltration. In particular, the last-mentioned process seems to be of special importance in the context of the climate induced disintegration of the ice shelves Larsen A and Larsen B (Scambos et al., 2000; NSIDC, 2002).

Conclusions

The basic objective of a series of diagnostic modelling studies on the LIS flow regime is to attain a description of its ice dynamics as comprehensively and accurately as possible. An initial reference run was carried out with an ordinary ice shelf model based on the generally used continuum-mechanical approach. However, the simulated ice dynamic situation shows considerable discrepancies from observed glacial conditions. Despite existing possibilities to improve model results (e.g., by solving the heat transfer equation to determine the temperature distribution in the ice body, by modifying boundary values, or by varying tuning-parameters like the flow enhancement factor m (cf. Rack et al., 2000; Scambos et al., 2000)), these discrepancies clearly show that important physical processes of high ice dynamical relevance cannot be simulated with the ordinary flow model. Above all, the arrangement and peculiarity of ice shelf fractures, which occur numerously in the LIS area, suggest the existence of zones of weakness within the ice body

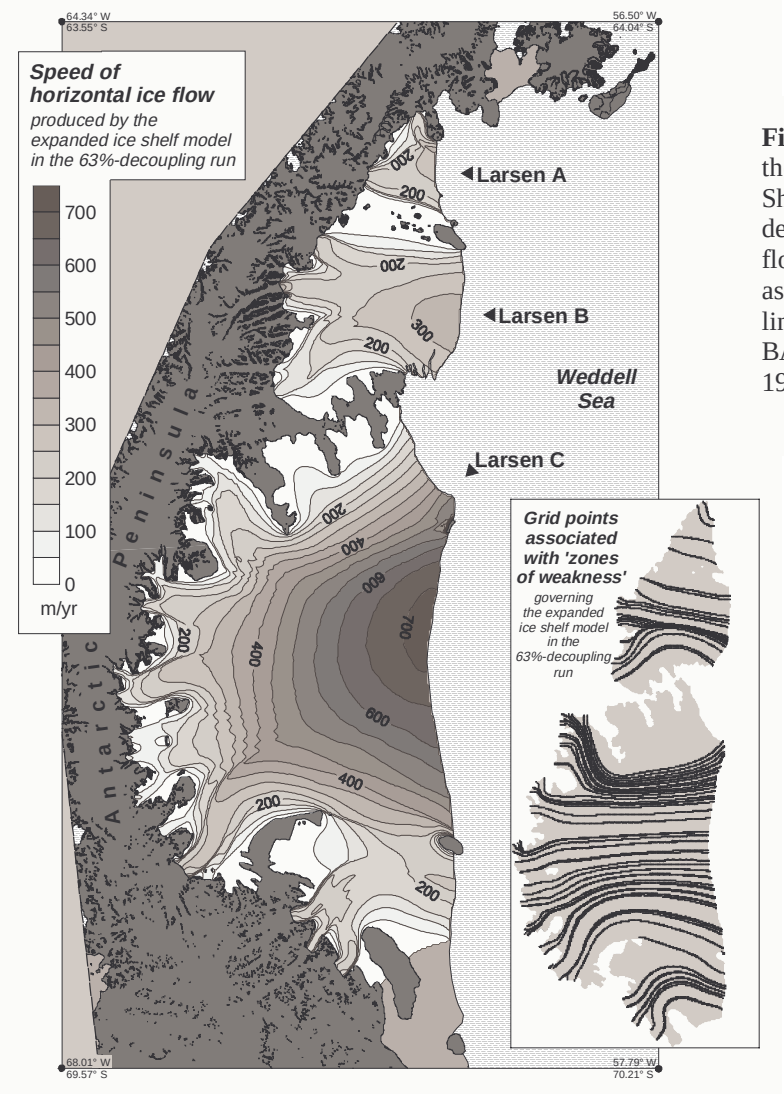

Figure 4: Modelled velocity field of the horizontal Larsen Ice Shelf flow. Shown are the results of the '63%-decoupling run' with the expanded flow model. The inset depicts the associated pattern of the considered lines of weakness. (Base of map: BAS et al., 1993; 1998; IOC et al., 1994)

connected with significant decoupling processes. Since to date neither direct evidence based on observations nor a physical quantitative characterisation of such failure zones is available, hypotheses have been put forward on how deep-reaching zones of weakness form and what their influence on the flow regime of the ice shelf might be. Thus, a parameterisation scheme was developed and implemented in the flow model. First results of the expanded ice shelf model, now being considerably more plausible from the ice dynamical point of view, highlight that a high-accuracy simulation of the flow regime requires the consideration of localised disintegrations of the mechanical integrity of the ice body and of decoupling processes associated with that. Besides, the newly developed parameterisation includes a couple of tuning-parameters and, therefore, offers the possibility for further improving the results. In the context of tuning-parameter adjustment, which implies the availability of a reliable data sets suited for validation purposes, the combination of ice dynamic modelling and satellite image data interferometry (cf. Rack et al., 2000) certainly comprises a great potential.

In order to scrutinise the general capability of the new parameterisation scheme and the whole expanded flow model, both diagnostic model applications for other ice shelves and time-dependent simulation studies are planed or have already been carried out (e.g., Saheicha et al., this issue).

References

Bamber, J.L. and P. Huybrechts (1996). Geometric boundary conditions for modelling the velocity field of the Antarctic ice sheet. *Ann. Glaciol*. **23**, 364-373.

BAS, SPRI, and WCMC (1993). *Antarctic digital database user's guide and reference manual*. Scientific Committee on Antarctic Research, Cambridge, U.K..

BAS, SPRI, and WCMC (1998). *Antarctic digital database, Version 2.0. Manual and bibliography*. Scientific Committee on Antarctic Research, Cambridge, U.K.

Bindschadler, R.A., M.A. Fahnestock, P. Skvarca, and T.A. Scambos (1994). Surface-velocity field of the northern Larsen Ice Shelf, Antarctica. *Ann. Glaciol*. **20**, 319-326.

Doake, C.S.M., H.F.J. Corr, H. Rott, P. Skvarca, and N.W. Young (1998). Breakup and conditions for stability of the northern Larsen Ice Shelf, Antarctica. *Nature* **391**, 778-780.

Herterich, K. (1987). On the flow within the transition zone between ice sheet and ice shelf. In: van der Veen, C.J. and J. Oerlemans (eds.), *Dynamics of the West Antarctic Ice Sheet*, D. Reidel Publishing Company, 185-202.

IOC, IHO, and BODC (1994). *The 'GEBCO Digital Atlas' including a CD-ROM*. Published on behalf of the Intergovernmental Oceanographic Commission (of Unesco) and the IHO as part of the GEBCO, British Oceanographic Data Centre (BODC), Birkenhead.

Jezek, K. and RAMP Product Team (2002). *RAMP AMM-1 SAR Image Mosaic of Antarctica*. Fairbanks, AK: Alaska SAR Facility, in association with the National Snow and Ice Data Center, Boulder, CO. Digital media.

Lythe, M.B., D.G. Vaughan, and the BEDMAP Consortium (2001). BEDMAP: A new ice thickness and subglacial topographic model of Antarctica. *J. Geophys. Res*. **106** (B6), 11,335-11,351.

MacAyeal, D.R., S. Shabtaie, C.R. Bentley, and S.D. King (1986). Formulation of ice shelf dynamic boundary conditions in terms of a Coulomb rheology. *J. Geophys. Res*. **91** (B8), 8177-8191.

NSIDC (2002). *Antarctic ice shelf collapses*. Antarctic ice shelves in the news at NSIDC, 19 March 2002, National Snow and Ice Data Center, University of Colorado, Boulder, http://www.nsidc.org/iceshelves/larsenb2002/index.html.

Paterson, W.S.B. (1994). *The physics of glaciers*. 3rd ed., Pergamon/Elsevier Science Ltd, Oxford, New York, Toronto.

Rack, W., H. Rott, A. Siegel, and P. Skvarca (1999). The motion field of northern Larsen Ice Shelf, Antarctic Peninsula, derived from satellite imagery. *Ann. Glaciol*. **29**, 261-266.

Rack, W., C.S.M. Doake, H. Rott, A. Siegel, and P. Skvarca (2000). Interferometric analysis of the deformation pattern of the northern Larsen Ice Shelf, Antarctic Peninsula, compared to field measurements and numerical modeling. *Ann. Glaciol*. **31**, 205-210.

Rott, H., P. Skvarca, and T. Nagler (1996). Rapid collapse of northern Larsen Ice Shelf, Antarctica. *Science* **271**, 788-792.

Rott, H., W Rack, T. Nagler, and P. Skvarca (1998). Climatically induced retreat and collapse of northern Larsen Ice Shelf, Antarctic Peninsula. *Ann. Glaciol*. **27**, 86-92.

Saheicha, K., H. Sandhäger, and M.A. Lange (2003). Numerical model studies to estimate the influence of fracture structures and zones of weakness on the flow regime of an idealized ice shelf system. In: Oerter, H. and L.H. Smedsrud (eds.): *Filchner-Ronne Ice Shelf Programme Report* **14**. Alfred Wegener Institute for Polar and Marine Research, Bremerhaven.

Scambos, T.A., C. Hulbe, M. Fahnestock, and J. Bohlander (2000). The link between climate warming and break-up of ice shelves in the Antarctic Peninsula. *J. Glaciol*. **46** (154), 516-530.

Skvarca, P. (1993). Fast recession of the northern Larsen Ice Shelf monitored by space images. *Ann. Glaciol*. **17**, 317-321.

Skvarca, P. (1994). Changes and surface features of the Larsen Ice Shelf, Antarctica, derived from Landsat and Kosmos mosaics. *Ann. Glaciol*. **20**, 6-12.

Skvarca, P., W. Rack, H. Rott, and T. Ibarzábal y Donángelo (1998). Evidence of recent climatic warming on the eastern Antarctic Peninsula. *Ann. Glaciol*. **27**, 628-632.

Skvarca, P., W. Rack, and H. Rott (1999). 34 year satellite time series to monitor characteristics, extent and dynamics of Larsen B Ice Shelf, Antarctic Peninsula. *Ann. Glaciol*. **29**, 255-260.

Vaughan, D.G. and C.S.M. Doake (1996). Recent atmospheric warming and retreat of ice shelves on the Antarctic Peninsula. *Nature* **379**, 328-331.